



## On the production of a $W$ and jets at hadron colliders

F.A. Berends, H. Kuijf and B. Tausk\*  
Instituut-Lorentz, University of Leiden,  
P.O.B. 9506, 2300 RA Leiden, The Netherlands.

W.T. Giele  
Fermi National Accelerator Laboratory,  
P.O.B. 500, Batavia, IL 60510, U.S.A.

October 1990

### Abstract

In this paper the evaluation of matrix elements for a vector boson decaying into  $n$  partons ( $n \leq 6$ ) is presented. For this purpose recursive techniques and Weyl-van der Waerden spinor calculus are used. By appropriately crossing partons the amplitudes can be used to describe the production of a  $W$  and jets. The four jet case is of particular interest as background to interesting physics signals. Numerical results are given for present and future accelerator energies. Also the signal versus background question for top quark search is briefly discussed.

---

\* Research supported by the Stichting F.O.M. \*



# 1 Introduction

In a previous paper analytic expressions were given [1] for processes involving a vector boson  $V$  and  $l$  partons. The number  $l$  was restricted to  $l \leq 5$ . An evaluation which was more numerically oriented has also been published [2]. Both approaches numerically agree [3].

In other words the decay

$$V \rightarrow l \text{ partons} \tag{1.1}$$

could be described in terms of the given expressions. By suitable crossing one obtains descriptions of

$$e^+ + e^- \rightarrow l \text{ jets}, \tag{1.2}$$

$$e^- + P \rightarrow \begin{pmatrix} e^- \\ \nu_e \end{pmatrix} + X + (l-1) \text{ jets}, \tag{1.3}$$

$$P + \begin{pmatrix} \bar{P} \\ P \end{pmatrix} \rightarrow X + V + (l-2) \text{ jets}. \tag{1.4}$$

It turns out that for a number of reasons the process (1.4) with  $l = 6$  is of particular interest. This has to do with its role as background to interesting physics signals.

The first signal is that of  $t\bar{t}$  production in a hadron collider, where one looks at the semileptonic  $t$  decay and at the quark decay of  $\bar{t}$ . When the mass of the  $t$  is large enough that the  $b$  is sufficiently energetic to develop into a jet, one has the signal  $e^+$  and four jets:

$$P + \begin{pmatrix} \bar{P} \\ P \end{pmatrix} \rightarrow X + t\bar{t} \rightarrow X + W^+ + W^- + b + \bar{b} \rightarrow X + e^+ + 4 \text{ jets}, \tag{1.5}$$

and similarly  $e^-$  and four jets. Obviously the QCD process (1.4) can be a serious background. For the top quark search at hadron colliders one shall be interested in the signal (1.5) besides the cleaner dilepton signal plus two jets arising from both  $W$ 's decaying leptonically.

The second signal of interest is that of heavy Higgs boson production by means of  $W$ -fusion, when one applies jet tagging [4].

$$\begin{aligned} P + P &\rightarrow X + q_1 + \bar{q}_2 + H \rightarrow X + q_1 + \bar{q}_2 + W^+ + W^- \\ &\rightarrow X + q_1 + \bar{q}_2 + e^\pm + q_3 + \bar{q}_4 \end{aligned} \tag{1.6}$$

Although the  $q_1$  and  $\bar{q}_2$  develop into jets relatively close to the beam direction one hopes to detect these jets. Again the process (1.4) will constitute a background. Of course signals other than (1.6) may give easier evidence for the Higgs boson (see e.g. [5]), but it would be worthwhile to study (1.6) as well.

For top masses below approximately 140 GeV the top quark could be found at the Tevatron in the near future and the knowledge of reaction (1.4) becomes rather relevant. When the top quark

N	Process type	# diagrams	# subprocesses
0	$u\bar{d}$	1	4
1	$u\bar{d}g$	2	12
2	$u\bar{d}gg$	8	14
	$u\bar{d}c\bar{c}$	2	52
	$u\bar{d}u\bar{u}$	4	14
	$u\bar{d}d\bar{d}$	4	14
3	$u\bar{d}ggg$	50	14
	$u\bar{d}c\bar{c}g$	12	92
	$u\bar{d}u\bar{u}g$	24	26
	$u\bar{d}d\bar{d}g$	24	26
4	$u\bar{d}gggg$	428	14
	$u\bar{d}c\bar{c}gg$	98	98
	$u\bar{d}u\bar{u}gg$	196	28
	$u\bar{d}d\bar{d}gg$	196	28
	$u\bar{d}c\bar{c}s\bar{s}$	16	108
	$u\bar{d}c\bar{c}c\bar{c}$	32	60
	$u\bar{d}u\bar{u}c\bar{c}$	32	98
	$u\bar{d}d\bar{d}c\bar{c}$	32	98
	$u\bar{d}u\bar{u}d\bar{d}$	64	28
	$u\bar{d}d\bar{d}d\bar{d}$	96	16
	$u\bar{d}u\bar{u}u\bar{u}$	96	16

Table 1. Counting statistics for the production of a  $W^+ \rightarrow e^+\nu$  in hadron colliders. N stands for the number of final state partons, Process type denotes the flavour combination, # diagrams is the number of Feynman diagrams of the process type and # subprocesses is the number of physical hadron-hadron collision processes producing a  $W^+$ . No mixing and no bottom in the initial state.

remains elusive at the Tevatron the signal and background question comes back again when LHC or SSC studies are made. For those accelerators also signal (1.6) and its background will have to be known.

Therefore we shall extend in this paper the previous calculations to  $l = 6$ . Although the formalism is set up in such a way that both W and Z could be considered, we shall focus on the W case, since that seems to be the most relevant case in view of the above signals.

The complexity of the process (1.1) rapidly increases with growing  $l$ . This is illustrated in table 1. In this table a typical parton combination is given and the number of subprocesses related to it using different flavour choices. Also the number of diagrams for the matrix element is listed. Let us take a specific case in order to indicate the meaning of the entries.

For the  $l = 4$  case in reaction (1.4) one has the following incoming parton combinations related to the generic  $u\bar{d}gg$  case:

$$u\bar{d} \rightarrow W^+gg, \tag{1.7}$$

$$ug \rightarrow W^+dg, \tag{1.8}$$

$$\bar{d}g \rightarrow W^+\bar{u}g, \tag{1.9}$$

$$gg \rightarrow W^+\bar{u}d. \tag{1.10}$$

Since the incoming hadrons contain four flavours, the cases (1.7)–(1.10) represent the following number of subprocesses: 4,4,4,2. Here we distinguish for example the  $u\bar{d}$  incoming state from  $\bar{d}u$ . The number of subprocesses is not the number of times a parton cross section has to be evaluated. This number is generally lower amongst others because different flavours can possess the same cross sections.

From the table it is clear that the  $l = 6$  case is considerably more complex than the  $l = 5$  case. Space limitations prevent us from listing explicitly analytic answers for helicity amplitudes as in the  $l = 5$  case. Nevertheless we shall give a description of the various kinds of amplitudes, i.e. 2, 4 and 6 quark matrix elements. The 2 quark matrix elements will be evaluated numerically with recursive techniques. The four quark matrix element calculation is similar to the  $l = 4$  and 5 cases as far as the quark structure is concerned. Of course the additional gluon adds to the complexity. The 6 quark case occurs here for the first time and is a generalization of the 4 quark case.

Besides a description of the calculation this paper also presents some numerical results for reaction (1.4), hereby extending the previous numbers [6] to the four jet case. The results for an increasing number of jets show a rather regular pattern, thus giving confidence in this complex evaluation. The results are for Tevatron, LHC and SSC situations. In a future paper we hope to present a more extensive phenomenological study for the Tevatron.

The actual outline of the paper is as follows. Section 2, 3 and 4 describe the 2, 4 and 6 quark amplitudes. Section 5 presents numerical results whereas section 6 summarizes the conclusions.

## 2 Matrix elements with one quark pair

In this section we deal with the calculation of the matrix elements involving a  $q\bar{q}$  pair, a vector boson and an arbitrary number of gluons. We choose for this case a different calculational technique than for the two and three quark pair cases. The reason is that when more gluons participate in a process, the number of diagrams increases rapidly. Therefore the calculation of helicity amplitudes by using Feynman diagrams becomes too complex, even when we use Weyl-van der Waerden spinor calculus. A technique recursive in the number of gluons has been introduced [7] for these situations. It pays off to use this technique when we have three or more gluons in a process, so for the one quark pair case we favour this approach.

After briefly summarizing those parts of the recursive calculation methods [7] required for the vector boson processes we look at the production of a  $W$  and at some numerical implications. We will show that for the process under consideration both the matrix element and the sum over the parton processes can be systematically dealt with for any number of gluons.

For the sake of presentation we consider the process with outgoing partons created from the vacuum

$$\emptyset \rightarrow V + q(Q; i) + \bar{q}(P; j) + g(K_1; a_1) + \dots + g(K_n; a_n). \quad (2.1)$$

The momenta and the colour indices are explicitly given. It is not of importance that process (2.1) is not a physical process. Later on we will cross two momenta from the final to the initial state. The matrix element for process (2.1) is given by a vector current  $\hat{S}_\mu(Q; 1 \dots n; P)$  contracted with the polarization vector  $V^\mu$  of the boson. For the sake of clarity we frequently omit colour and momentum indices in  $\hat{S}_\mu$ , they are implicitly understood. In [1] process (2.1) is discussed in great detail. Here we only present the main elements of the method to obtain  $\hat{S}_\mu$ .

The vector boson couples to the quark line breaking the Feynman diagram into two parts, one spinor current with the  $q(Q)$  and gluons 1 through  $m$  and one spinor current with  $\bar{q}(P)$  and the rest of the gluons,  $m + 1$  through  $n$ . These two spinor currents can be decomposed in a colour base of fundamental representation matrices  $T^a$  of the  $SU(N)$  colour gauge group. The spinor currents are given by

$$\hat{J}(Q; 1 \dots m) = g^m \sum_{P(1 \dots m)} (T^{a_1} \dots T^{a_m})_{ik} J(Q; 1 \dots m) \quad (2.2)$$

and

$$\hat{J}(m + 1 \dots n; P) = g^{n-m} \sum_{P(m+1 \dots n)} (T^{a_{m+1}} \dots T^{a_n})_{kj} J(m + 1 \dots n; P), \quad (2.3)$$

where the sum is over all gluon permutations. The quark currents  $J(Q; 1 \dots m)$  and  $J(m + 1 \dots n; P)$  are calculated using recursion in the number of gluons [7]. For the no gluon case they are:  $J(Q) = \bar{u}(Q)$  and  $J(P) = v(P)$ . Using eqs. (2.2) and (2.3)  $\hat{S}_\mu$  can be written as

$$\hat{S}_\mu(Q; 1 \dots n; P) = ie g^n \sum_{P(1 \dots n)} (T^{a_1} \dots T^{a_n})_{ij} S_\mu(Q; 1 \dots n; P) \quad (2.4)$$

with

$$S_\mu(Q; 1 \dots n; P) = \sum_{m=0}^n J(Q; 1 \dots m) \Gamma_\mu^{V, f_1, f_2} J(m + 1 \dots n; P). \quad (2.5)$$

Eqs. (2.4) and (2.5) reflect the coupling of the vector boson at all possible positions on the quark line with the gluons randomly distributed over both sides. The vertex  $\Gamma_\mu^{V, f_1, f_2}$  depends on the nature of the vector boson and on the quark flavours. Throughout this paper we set the KM matrix equal to unity. This has very little influence on the results [6]. All the  $S_\mu$ 's are conserved quantities,

$$S_\mu(Q; 1 \dots n; P)(Q + K_1 + \dots + K_n + P)^\mu = 0. \quad (2.6)$$

They are also gauge invariant in the sense that replacing a gluon polarization vector  $J(i)$  by the momentum  $K_i$  gives zero. The matrix element is given by

$$\mathcal{M}(Q; 1, 2, \dots, n; P) = V^\mu \hat{S}_\mu. \quad (2.7)$$

The computation of the matrix element squared  $|V^\mu \hat{S}_\mu|^2$  is done as follows. First determine all the  $S_\mu$ 's using eq. (2.5). The fact that we let the vector boson decay has two consequences. The first is that we have to include a propagator for it. Thus one has

$$V^\mu = \frac{-ig^{\mu\nu}}{s - M_V^2 + iM_V\Gamma_V} L_\nu. \quad (2.8)$$

In this formula,  $s$ ,  $M_V$  and  $\Gamma_V$  are the momentum squared, the mass and the width of the vector boson, respectively, and  $L_\nu$  is a lepton current, which is given by

$$L_\nu = ie\bar{u}(l_1)\Gamma_\nu^{V,l_1l_2}v(l_2). \quad (2.9)$$

Secondly the vector boson decays into two massless particles and therefore we only need to sum over the two polarization states which correspond to the  $+-$  and  $-+$  spin states of the decay products. Finally the square  $|V^\mu \hat{S}_\mu|^2$  contains a colour matrix which originates from the product of the colour parts. We work out those products with

$$(T^a)_{ij}(T^a)_{kl} = \frac{1}{2} [\delta_{ij}\delta_{kl} - \delta_{ij}\delta_{kl}/N] \quad (2.10)$$

resulting in a polynomial in  $N$ . This procedure has to be repeated for all possible helicity configurations of the quarks, gluons and the decay products of the vector boson. The method sketched above is valid for any number of gluons. Only the colour matrix has to be determined separately for each value of  $n$ .

Specifying that the vector boson is a  $W$  leads to a reduction in the number of helicity amplitudes that has to be evaluated because the  $W$  only couples left-handedly. When implemented numerically the general recursive method can very well compete with analytical results as far as numerical evaluation speed is concerned. In table 2 we made a comparison between two programs, one based on the analytical results of [1] and one based on the numerical recursion method. One can see that there is not much difference in the CPU-times needed. Together with the fact that for  $n \geq 3$  the analytical results are very hard to obtain it shows that the recursive approach is the method to use.

In the physical situation where we consider  $P\bar{P} \rightarrow V + \text{jets}$ , two of the QCD particles in process (2.1) have to be crossed from the final to the initial state. There are four possible ways :

$$q(P)\bar{q}(Q) \rightarrow V + g(K_1) + \dots + g(K_n) \quad n \geq 0 \quad (2.11)$$

$$q(P)g(K_1) \rightarrow V + q(Q) + g(K_2) + \dots + g(K_n) \quad n \geq 1 \quad (2.12)$$

$$\bar{q}(Q)g(K_1) \rightarrow V + \bar{q}(P) + g(K_2) + \dots + g(K_n) \quad n \geq 1 \quad (2.13)$$

$$g(K_1)g(K_2) \rightarrow V + q(Q) + \bar{q}(P) + g(K_3) + \dots + g(K_n) \quad n \geq 2 \quad (2.14)$$

Nr. Gluons	W/Z old	W/Z new
0	0.00226	0.00223
1	0.00404	0.00386
2	0.01168	0.01233
3	0.1046	0.0807
4	—	0.8908
5	—	14.580

Table 2. CPU-time in seconds of the W/Z matrix elements with a quark pair and  $n$  gluons. Old entry stands for the routines based on [1]. New entry is the general method with recursion. Timing on a VAX 3500.

In the case  $n \geq 2$  four different matrix elements have to be evaluated. The fact that for more final state particles the extra gluon always ends up in the final state of the four processes mentioned above enables us to write down a general algorithm for the sum over physical subprocesses.

### 3 Matrix elements with two quark pairs

Here we discuss the calculation of the tree level matrix elements for the creation of a vector boson, two quarks, two antiquarks and two gluons, followed by the decay of the vectorboson into a lepton pair:

$$\emptyset \rightarrow V q_1 \bar{q}_2 q_3 \bar{q}_4 g_1 g_2, \quad V \rightarrow l_1 \bar{l}_2. \quad (3.1)$$

Again we get the matrix elements for physical processes that occur in collision experiments by crossing two particles to the initial state. In contrast to the previous section we use explicit Feynman diagrams which will be grouped in gauge invariant sets. Helicity amplitudes will eventually be obtained from them with help of Weyl-van der Waerden spinor calculus.

The matrix element  $\mathcal{M}$  is given by

$$\mathcal{M} = V^\mu \hat{T}_\mu, \quad (3.2)$$

where  $V^\mu$  is given by eq. (2.8). From now on, we focus on the calculation of the four quark, two gluon coloured current  $\hat{T}_\mu$ . All quarks are assumed to be massless.

For the (anti-)quarks we will use the symbol  $Q_i$ , which stands for  $(Q_i, \lambda_{q_i}, c_i, f_i)$ , with  $Q_i$  = momentum,  $\lambda_{q_i}$  = helicity,  $c_i$  = colour and  $f_i$  = flavour. We denote the gluons by 1 and 2, which stand for  $(K_i, \lambda_{g_i}, a_i)$ , ( $i = 1, 2$ ), with  $K_i$  = momentum,  $\lambda_{g_i}$  = helicity and  $a_i$  = colour.

The calculation of the current  $\hat{T}_\mu$  is in many ways similar to that of the  $q\bar{q}q\bar{q}$  and  $q\bar{q}q\bar{q}g$  currents presented in [1]. We will use several definitions, and also some results given there.

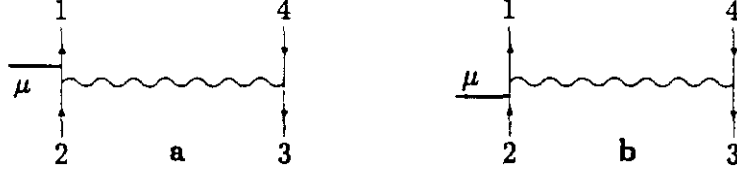


Fig. 1. The two basic diagrams for the four quark process.

First, we write  $\hat{T}_\mu$  as the sum of four parts  $\hat{A}_\mu$ :

$$\begin{aligned} \hat{T}_\mu(Q_1 Q_2 Q_3 Q_4; 12) &= \hat{A}_\mu(Q_1 Q_2 Q_3 Q_4; 12) - \hat{A}_\mu(Q_3 Q_2 Q_1 Q_4; 12) \\ &- \hat{A}_\mu(Q_1 Q_4 Q_3 Q_2; 12) + \hat{A}_\mu(Q_3 Q_4 Q_1 Q_2; 12). \end{aligned} \quad (3.3)$$

$\hat{A}_\mu(Q_1 Q_2 Q_3 Q_4; 12)$  is the sum of all Feynman diagrams that can be constructed by attaching two gluons  $g_1$  and  $g_2$  to the two basic diagrams in fig. 1. We will refer to the diagrams constructed using the left diagram as a-type diagrams and to the ones using the right diagram as b-type diagrams.

By combining the colour matrices associated with the vertices of a particular diagram using eq. (2.10), we can write it as the product of a colour factor and a colour independent factor. Doing this for all diagrams we find that the following factors occur:

$$\gamma_1(c_1 c_2 c_3 c_4; a_1 a_2) = \delta_{c_1 c_4} (T^{a_1} T^{a_2})_{c_3 c_2} \quad (3.4)$$

$$\gamma_2(c_1 c_2 c_3 c_4; a_1 a_2) = (T^{a_1})_{c_1 c_4} (T^{a_2})_{c_3 c_2}. \quad (3.5)$$

$$\gamma_3(c_1 c_2 c_3 c_4; a_1 a_2) = (T^{a_1} T^{a_2})_{c_1 c_4} \delta_{c_3 c_2} \quad (3.6)$$

$$\gamma_4(c_1 c_2 c_3 c_4; a_1 a_2) = -\frac{1}{N} \delta_{c_1 c_2} (T^{a_1} T^{a_2})_{c_3 c_4} \quad (3.7)$$

$$\gamma_5(c_1 c_2 c_3 c_4; a_1 a_2) = -\frac{1}{N} (T^{a_1})_{c_1 c_2} (T^{a_2})_{c_3 c_4} \quad (3.8)$$

$$\gamma_6(c_1 c_2 c_3 c_4; a_1 a_2) = -\frac{1}{N} (T^{a_1} T^{a_2})_{c_1 c_2} \delta_{c_3 c_4} \quad (3.9)$$

$$\gamma_{i+6}(c_1 c_2 c_3 c_4; a_1 a_2) = \gamma_i(c_1 c_2 c_3 c_4; a_2 a_1) \text{ for } i = 1, \dots, 6. \quad (3.10)$$

Splitting off the colour factors, and using the invariance of  $\hat{A}_\mu$  when  $g_1$  and  $g_2$  are interchanged, we obtain:

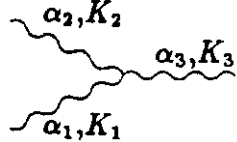
$$\begin{aligned} \hat{A}_\mu(Q_1 Q_2 Q_3 Q_4; 12) &= \\ &ieg^4 \delta^{f_3 f_4} \sum_{P(12)} \sum_{i=1}^6 \gamma_i(c_1 c_2 c_3 c_4; a_1 a_2) B_{i\mu}^{f_1 f_2}(Q_1 Q_2 Q_3 Q_4; 12). \end{aligned} \quad (3.11)$$

The sum is over the two possible orders of the gluons. A common factor  $ieg^4 \delta^{f_3 f_4}$  has also been extracted.

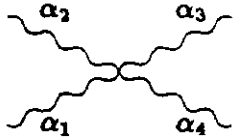


Before proceeding to describe the calculation of the functions  $B_{i\mu}^{f_1 f_2}$ , we note that  $\hat{A}_\mu$  is gauge invariant, i.e. it vanishes when a gluon polarization vector  $J_\mu$  is replaced by its momentum  $K_\mu$ . Because the colour factors  $\gamma_i$  are independent, this means that the  $B_{i\mu}^{f_1 f_2}$ 's are also gauge invariant. Our strategy is to divide the  $B_{i\mu}^{f_1 f_2}$ 's into as many gauge invariant pieces as possible and then to calculate all those pieces separately, choosing the most convenient gauge for the gluon polarization vectors in each piece.

We will give a description of the Feynman graphs that contribute to the  $B_{i\mu}$ 's. They are now colourless diagrams. The meaning of the three and four gluon vertices is as follows:



$$igV^{\alpha_1\alpha_2\alpha_3}(K_1, K_2, K_3) = ig[(K_1 - K_2)^{\alpha_3} g^{\alpha_1\alpha_2} + (K_2 - K_3)^{\alpha_1} g^{\alpha_2\alpha_3} + (K_3 - K_1)^{\alpha_2} g^{\alpha_3\alpha_1}]. \quad (3.12)$$



$$ig^2 [2g^{\alpha_1\alpha_3} g^{\alpha_2\alpha_4} - g^{\alpha_1\alpha_2} g^{\alpha_3\alpha_4} - g^{\alpha_1\alpha_4} g^{\alpha_2\alpha_3}]. \quad (3.13)$$

These vertices are not symmetric under permutations of the gluons, so to have an unambiguous correspondence between the diagrams and the formulae, we adopt the convention that the gluons with labels (1, 2, 3) in eq. (3.12) must be arranged in ascending order when one goes around the diagram clockwise. Similarly, for the four gluon vertex, the gluons labeled (1, 2, 3, 4) in (3.13) must be arranged clockwise around the diagram.

Let us begin with  $B_{4\mu}$ ,  $B_{5\mu}$  and  $B_{6\mu}$ , since they are somewhat simpler than  $B_{1\mu}$ ,  $B_{2\mu}$  and  $B_{3\mu}$ . We shall derive some expressions for them consisting of parts which we already know from [1] and new quantities. For the latter we don't give the explicit results but we indicate which type of diagrams contribute. Also the occurrence of gauge invariant subsets is noticed for the reasons mentioned above.

The diagrams for  $B_{4\mu}$  are obtained by attaching  $g_1$  and  $g_2$  to the quark line that connects  $Q_3$  with  $Q_4$  in diagram a or diagram b. Gluon 1 must be attached below gluon 2. In other words, if we follow the quark line from  $Q_3$  up towards  $Q_4$ , we should reach  $g_1$  before we reach  $g_2$ .  $B_{4\mu}$  also contains the diagrams where  $g_1$  and  $g_2$  are connected to each other by a three gluon vertex which is connected to the  $Q_3 - Q_4$  quark line. By adding all the diagrams we obtain:

$$B_{4\mu}^{f_1 f_2}(Q_1 Q_2 Q_3 Q_4; 12) = \frac{1}{2} S_{\mu\alpha}^{V, f_1 f_2}(Q_1; Q_2) \frac{g^{\alpha\beta}}{(Q_3 + Q_4 + K_1 + K_2)^2} S_\beta(Q_3; 12; Q_4), \quad (3.14)$$

with

$$\begin{aligned} S_{\mu\alpha}^{V, f_1 f_2}(Q_1; Q_2) &= J(Q_1) \Gamma_\mu^{V, f_1 f_2} [Q_1 + Q_2 + Q_3 + K_1 + K_2]^{-1} \gamma_\alpha J(Q_2) \\ &- J(Q_1) \gamma_\alpha [Q_1 + Q_2 + Q_3 + K_1 + K_2]^{-1} \Gamma_\mu^{V, f_1 f_2} J(Q_2) \end{aligned} \quad (3.15)$$

and  $S_\beta(Q_3; 12; Q_4)$  as in eq. (2.5), but now with  $\Gamma_\mu^{V, f_1 f_2}$  replaced by  $\gamma_\beta$ . By inserting only the first term of eq. (3.15) in eq. (3.14) instead of the whole  $S_{\mu\alpha}^{V, f_1 f_2}$ , we obtain a quantity we call  $B_{4\mu\alpha}$ . It is precisely the sum of all the a-type diagrams in  $B_{4\mu}$ . Taking only the second term of eq. (3.15) we get  $B_{4\mu b}$ , the sum of all the b-type diagrams. From the gauge invariance of  $S_\beta$  we infer that  $B_{4\mu\alpha}$  and  $B_{4\mu b}$  are both gauge invariant.

When translated into Weyl-van der Waerden spinor language, eq. (3.14) and eq. (3.15) become:

$$B_{4\mu}^{f_1 f_2}(Q_1^+ Q_2^- Q_3 Q_4; 12) = \frac{(\sqrt{2})^2 R^{V, f_1 f_2} \sigma_\mu^{AB} S_{AB\dot{C}D}^V(Q_1^+ Q_2^-) S^{\dot{C}D}(Q_3; 12; Q_4)}{(Q_3 + Q_4 + K_1 + K_2)^2} \quad (3.16)$$

$$B_{4\mu}^{f_1 f_2}(Q_1^- Q_2^+ Q_3 Q_4; 12) = \frac{(\sqrt{2})^2 L^{V, f_1 f_2} \sigma_\mu^{AB} S_{AB\dot{C}D}^V(Q_1^- Q_2^+) S^{\dot{C}D}(Q_3; 12; Q_4)}{(Q_3 + Q_4 + K_1 + K_2)^2} \quad (3.17)$$

with

$$\begin{aligned} S_{AB\dot{C}D}^V(Q_1^+ Q_2^-) &= \frac{g_{1A}(Q_2 + Q_3 + Q_4 + K_1 + K_2) \dot{C}_B Q_{2D}}{(Q_2 + Q_3 + Q_4 + K_1 + K_2)^2} \\ &- \frac{g_{1\dot{C}}(Q_1 + Q_3 + Q_4 + K_1 + K_2) A_D Q_{2B}}{(Q_1 + Q_3 + Q_4 + K_1 + K_2)^2} \end{aligned} \quad (3.18)$$

and

$$S_{AB\dot{C}D}^V(Q_1^- Q_2^+) = -S_{AB\dot{C}D}^V(Q_2^+ Q_1^-). \quad (3.19)$$

The quantities  $L^{V, f_1 f_2}$  and  $R^{V, f_1 f_2}$  are the coupling constants in

$$\Gamma_\mu^{V, f_1 f_2} = L^{V, f_1 f_2} \gamma_\mu \left( \frac{1 - \gamma_5}{2} \right) + R^{V, f_1 f_2} \gamma_\mu \left( \frac{1 + \gamma_5}{2} \right). \quad (3.20)$$

$S_{AB}(Q_3; 12; Q_4)$  is defined by

$$S_\beta(Q_3; 12; Q_4) = (\sqrt{2})^2 \sigma_\beta^{AB} S_{AB}(Q_3; 12; Q_4). \quad (3.21)$$

Expressions for  $S_{AB}(Q_3; 12; Q_4)$  are listed in [1].

The diagrams for  $B_{5\mu}$  have  $g_1$  attached to the left quark line and  $g_2$  attached to the right quark line. Their sum can be expressed as a product in a way similar to  $B_{4\mu}$ :

$$\begin{aligned} B_{5\mu}^{f_1 f_2}(Q_1 Q_2 Q_3 Q_4; 12) &= \\ &\frac{1}{2} S_{\mu\alpha}^{V, f_1 f_2}(Q_1; 1; Q_2) \frac{g^{\alpha\beta}}{(Q_3 + Q_4 + K_2)^2} S_\beta(Q_3; 2; Q_4). \end{aligned} \quad (3.22)$$

$S_{\mu\alpha}^{V,f_1f_2}$  is the sum of six diagrams:

$$S_{\mu\alpha}^{V,f_1f_2}(Q_1; 1; Q_2) = \quad (3.23)$$

$$\begin{aligned} &+ J(Q_1; 1) \Gamma_{\mu}^{V,f_1f_2}[\not{d}]^{-1} \gamma_{\alpha} J(Q_2) \\ &+ J(Q_1) \Gamma_{\mu}^{V,f_1f_2}[\not{d} + K_1]^{-1} \not{d}(1)[\not{d}]^{-1} \gamma_{\alpha} J(Q_2) \\ &+ J(Q_1) \Gamma_{\mu}^{V,f_1f_2}[\not{d} + K_1]^{-1} \gamma_{\alpha} J(1; Q_2) \\ &- J(Q_1; 1) \gamma_{\alpha} [\not{d} + K_1]^{-1} \Gamma_{\mu}^{V,f_1f_2} J(Q_2) \\ &+ J(Q_1) \gamma_{\alpha} [\not{d}]^{-1} \not{d}(1) [\not{d} + K_1]^{-1} \Gamma_{\mu}^{V,f_1f_2} J(Q_2) \\ &- J(Q_1) \gamma_{\alpha} [\not{d}]^{-1} \Gamma_{\mu}^{V,f_1f_2} J(1; Q_2), \end{aligned} \quad (3.24)$$

where the abbreviations  $a = Q_2 + Q_3 + Q_4 + K_2$  and  $b = Q_1 + Q_3 + Q_4 + K_2$  have been used.  $B_{5\mu}$  is the sum of two gauge invariant parts,  $B_{5\mu a}$  and  $B_{5\mu b}$ , which consist of all the a-type and b-type diagrams, respectively. This corresponds to separating the first three terms and the last three terms in eq. (3.23). Translating eq. (3.22) into spinor language using

$$S_{\mu\alpha}^{V,f_1f_2}(Q_1^+; 1; Q_2^-) = \sqrt{2} \sigma_{\mu}^{AB} \sigma_{\alpha}^{CD} R^{V,f_1f_2} S_{\dot{A}B\dot{C}D}^V(Q_1^+; 1; Q_2^-), \quad (3.25)$$

$$S_{\mu\alpha}^{V,f_1f_2}(Q_1^-; 1; Q_2^+) = \sqrt{2} \sigma_{\mu}^{AB} \sigma_{\alpha}^{CD} L^{V,f_1f_2} S_{\dot{A}B\dot{C}D}^V(Q_1^-; 1; Q_2^+), \quad (3.26)$$

and

$$S_{\beta}(Q_3; 2; Q_4) = \sqrt{2} \sigma_{\beta}^{AB} S_{\dot{A}B}(Q_3; 2; Q_4) \quad (3.27)$$

we find

$$B_{5\mu}^{f_1f_2}(Q_1^+ Q_2^- Q_3 Q_4; 12) = \frac{(\sqrt{2})^2 R^{V,f_1f_2} \sigma_{\mu}^{AB} S_{\dot{A}B\dot{C}D}^V(Q_1^+; 1; Q_2^-) S^{\dot{C}D}(Q_3; 2; Q_4)}{(Q_3 + Q_4 + K_2)^2} \quad (3.28)$$

$$B_{5\mu}^{f_1f_2}(Q_1^- Q_2^+ Q_3 Q_4; 12) = \frac{(\sqrt{2})^2 L^{V,f_1f_2} \sigma_{\mu}^{AB} S_{\dot{A}B\dot{C}D}^V(Q_1^-; 1; Q_2^+) S^{\dot{C}D}(Q_3; 2; Q_4)}{(Q_3 + Q_4 + K_2)^2}. \quad (3.29)$$

Expressions for  $S_{\dot{A}B}(Q_3; 2; Q_4)$  can be found in [1].  $S_{\dot{A}B\dot{C}D}^V$  must be calculated for each helicity combination. Although eq. (3.23) contains six terms, the number of terms in  $S_{\dot{A}B\dot{C}D}^V$  can be reduced to four by using an appropriate gauge.

The next function,  $B_{6\mu}$ , is treated in the same way. The diagrams for  $B_{6\mu}$  have  $g_1$  and  $g_2$  both attached to the left quark line of diagram a or diagram b, with  $g_1$  nearest to  $Q_1$  and  $g_2$  nearest to  $Q_2$

$$\begin{aligned} B_{6\mu}^{f_1f_2}(Q_1 Q_2 Q_3 Q_4; 12) = \\ \frac{1}{2} S_{\mu\alpha}^{V,f_1f_2}(Q_1; 12; Q_2) \frac{g^{\alpha\beta}}{(Q_3 + Q_4)^2} S_{\beta}(Q_3; Q_4). \end{aligned} \quad (3.30)$$

Here  $S_{\mu\alpha}^{V,f_1f_2}(Q_1; 12; Q_2)$  is defined analogously to  $S_{\mu\alpha}^{V,f_1f_2}(Q_1; 1; Q_2)$  and  $S_{\mu\alpha}^{V,f_1f_2}(Q_1; Q_2)$ . It contains contributions from 18 diagrams and it has to be calculated for every helicity combination. Once again, the a-type part  $B_{6,\mu a}$  and the b-type part  $B_{6,\mu b}$  are separately gauge invariant.

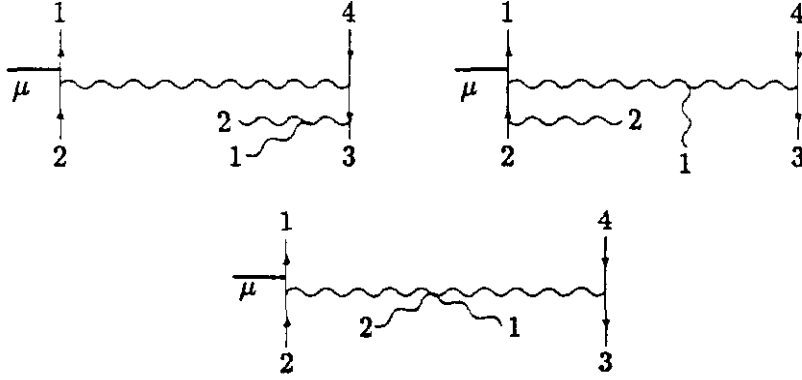


Fig. 2. Examples of diagrams for  $B_{1\mu}$ .

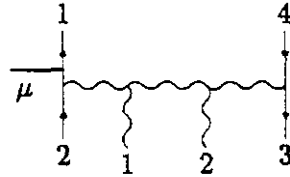


Fig. 3. This diagram does not contribute to  $B_{1\mu}$ .

The other  $B$ -functions,  $B_{1\mu}$ ,  $B_{2\mu}$  and  $B_{3\mu}$ , will now be discussed. The diagrams for  $B_{1\mu}$  are obtained by adding  $g_1$  and  $g_2$  on to the bottom of diagram a or diagram b, i.e. they must be connected to the diagram somewhere along the line which starts at  $Q_3$  and goes to  $Q_2$ . Someone travelling along that line should meet  $g_1$  before he meets  $g_2$ . There are 25 diagrams of this kind. Some examples are shown in fig. 2. The quarks and gluons, starting from  $Q_1$  and going clockwise, are arranged in the order  $Q_1Q_4Q_312Q_2$ . Note that the colour labels in the colour factor (3.4) occur in the same order, i.e.  $c_1c_4c_3a_1a_2c_2$  (reading the labels of a string  $(T^aT^b\dots T^k)_{xy}$  in the order  $xab\dots ky$ ). On the other hand the diagram in fig. 3 has  $g_1$  and  $g_2$  in the wrong order and should not be considered for  $B_{1\mu}$ .

The connection between diagrams and their colour factors is a general feature of all colour structures. For  $B_{2\mu}$  there are 28 diagrams. They have  $g_1$  attached to the top of the diagram, somewhere between  $Q_1$  and  $Q_4$ , and  $g_2$  attached to the bottom, like for example fig. 4. The diagrams for  $B_{3\mu}$  have both  $g_1$  and  $g_2$  attached on the top, with  $g_1$  to the left of  $g_2$ . The number of diagrams is again 25 and there is, in fact, a one to one correspondence between the diagrams of  $B_{1\mu}$  and those of  $B_{3\mu}$ . This is an instance of a more general symmetry of  $\hat{A}_\mu$ , which follows from CP invariance, that we will discuss later on. It can be exploited to derive  $B_{3\mu}$  from  $B_{1\mu}$ , once the latter has been calculated.

Simply separating the a-type and b-type contributions, as we did with  $B_{4\mu}$ ,  $B_{5\mu}$  and  $B_{6\mu}$ , does not yield gauge invariant parts of  $B_{1\mu}$ ,  $B_{2\mu}$  and  $B_{3\mu}$ . This is due to diagrams like eg. fig. 4, which have one or more gluons attached to the internal gluon of diagram a or diagram b. When we take diagrams like that and replace  $J_\mu$  by  $K_\mu$ , we do not get zero unless we take the a-type and the b-type diagrams all together. However, we can find gauge invariant parts in a slightly more complicated way. For this, we first take a look at the expression for diagram a:

$$\frac{1}{2}J(Q_1)\Gamma_\mu^{V, f_1 f_2}[\mathcal{Q}_2 + \mathcal{Q}_3 + \mathcal{Q}_4]^{-1}\gamma_\alpha J(Q_2)\frac{g^{\alpha\beta}}{(Q_3 + Q_4)^2}J(Q_3)\gamma_\beta J(Q_4). \quad (3.31)$$

It contains a  $\gamma_\alpha$  on the left quark line and a  $\gamma_\beta$  on the right quark line, connected by the metric tensor  $g^{\alpha\beta}$ . All the diagrams for  $B_{4\mu}$ ,  $B_{5\mu}$  and  $B_{6\mu}$  contain this factor, but in diagrams where gluons are attached to the internal gluon of diagram a or diagram b, there is a more complicated tensor in between  $\gamma_\alpha$  and  $\gamma_\beta$ .

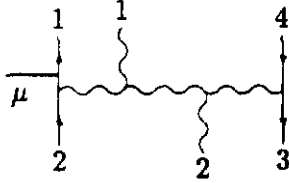


Fig. 4. A contribution to  $B_{2\mu}$ .

For example in fig. 4 it is:

$$J(1)_\nu V^{\alpha\nu\kappa}(-Q_3 + Q_4 + K_1 + K_2, K_1, Q_3 + Q_4 + K_2) \times g_{\kappa\lambda} V^{\lambda\beta\rho}(-Q_3 + Q_4 + K_2, Q_3 + Q_4, K_2) J(2)_\rho. \quad (3.32)$$

When we substitute eq. (3.12) in eq. (3.32) and contract all the dummy indices we find, among many other terms, one that is proportional to  $g^{\alpha\beta}$ . This happens in all the other diagrams as well. The quantity containing all contributions to  $B_{1\mu}$  that are proportional to  $g^{\alpha\beta}$ , is gauge invariant. Let us call it " $B_{1\mu}(g^{\alpha\beta})$ " for the moment. Of course, the rest of  $B_{1\mu}$ , " $B_{1\mu}(\text{no } g^{\alpha\beta})$ ", is also gauge invariant. Within  $B_{1\mu}(g^{\alpha\beta})$  we can still separate the a-type and the b-type contributions, but in  $B_{1\mu}(\text{no } g^{\alpha\beta})$  we cannot. So, our final decomposition of  $B_{1\mu}$  is:

$$\begin{aligned} B_{1\mu} &= B_{1\mu a} + B_{1\mu b} + B_{1\mu c} \text{ with} \\ B_{1\mu a} &= \text{sum of a-type contributions proportional to } g^{\alpha\beta}, \\ B_{1\mu b} &= \text{sum of b-type contributions proportional to } g^{\alpha\beta}, \\ B_{1\mu c} &= \text{everything else.} \end{aligned} \quad (3.33)$$

The quantities  $B_{2\mu}$  and  $B_{3\mu}$  are decomposed in exactly the same way.

To calculate the currents  $B_{i\mu}$ , two methods are used. The first is to take a gauge invariant quantity and use Weyl-van der Waerden formalism for an immediate evaluation, choosing gauge spinors

for the gluons that make this as easy as possible. When we use the second method, we postpone the specification of the helicities and the introduction of Weyl-van der Waerden spinors. First we combine terms so that we end up with formulae that no longer contain any gluon polarization vectors explicitly, but only implicitly through the abelian field strengths  $F^{\mu\nu} = K^\mu J^\nu - K^\nu J^\mu$ . After that, we proceed in the normal way, expressing everything in terms of spinors, except that this time there is no need to choose gauge spinors, since  $F^{\mu\nu}$  is manifestly gauge invariant. Sometimes, it is convenient to use a combination of the two methods.

To test the results we performed several numerical checks, which are based on the following properties of the  $B$ -functions.

The first is current conservation:

$$(Q_1 + Q_2 + Q_3 + Q_4 + K_1 + K_2)^\mu B_{i\mu} = 0. \quad (3.34)$$

Then there is a set of relationships that can be proved using charge conjugation invariance.

$$\begin{aligned} B_{1\mu}^{f_1 f_2}(Q_1 Q_2 Q_3 Q_4; 12) &= -\tilde{B}_{3\mu}^{f_2 f_1}(Q_2 Q_1 Q_4 Q_3; 21) \\ B_{2\mu}^{f_1 f_2}(Q_1 Q_2 Q_3 Q_4; 12) &= -\tilde{B}_{2\mu}^{f_2 f_1}(Q_2 Q_1 Q_4 Q_3; 21) \\ B_{4\mu}^{f_1 f_2}(Q_1 Q_2 Q_3 Q_4; 12) &= -\tilde{B}_{4\mu}^{f_2 f_1}(Q_2 Q_1 Q_4 Q_3; 21) \\ B_{5\mu}^{f_1 f_2}(Q_1 Q_2 Q_3 Q_4; 12) &= -\tilde{B}_{5\mu}^{f_2 f_1}(Q_2 Q_1 Q_4 Q_3; 12) \\ B_{6\mu}^{f_1 f_2}(Q_1 Q_2 Q_3 Q_4; 12) &= -\tilde{B}_{6\mu}^{f_2 f_1}(Q_2 Q_1 Q_4 Q_3; 21) \end{aligned} \quad (3.35)$$

The wiggle above the  $B$ -functions on the right hand side means that they must be calculated with the vector boson vertex (3.20) replaced by

$$\tilde{\Gamma}_\mu^{V, f_1 f_2} = R^{V, f_1 f_2} \gamma_\mu \left( \frac{1 - \gamma_5}{2} \right) + L^{V, f_1 f_2} \gamma_\mu \left( \frac{1 + \gamma_5}{2} \right). \quad (3.36)$$

In certain regions of phase space the  $B$ -functions diverge because they contain diagrams with denominators that vanish. This happens when the energy of one of the gluons goes to zero, and also, because we are neglecting quark masses, when particles are collinear. In these limits, our tree level calculation is certainly not a good approximation to the exact S-matrix element. Nevertheless, it is useful to evaluate the  $B$ -functions numerically in the soft and collinear limits, because asymptotically, they can be related to currents  $B_\mu$  and  $S_\mu$  that have been calculated and checked before [1].

The soft limits that were tested are the limit when  $g_1$  becomes soft:

$$B_{1\mu}^{f_1 f_2}(Q_1 Q_2 Q_3 Q_4; g_1 g_2) \rightarrow S_{Q_3 \underline{K}_1 K_2} B_{1\mu}^{f_1 f_2}(Q_1 Q_2 Q_3 Q_4; g_2), \quad (3.37)$$

$$B_{2\mu}^{f_1 f_2}(Q_1 Q_2 Q_3 Q_4; g_1 g_2) \rightarrow S_{Q_1 \underline{K}_1 Q_4} B_{2\mu}^{f_1 f_2}(Q_1 Q_2 Q_3 Q_4; g_2), \quad (3.38)$$

$$B_{3\mu}^{f_1 f_2}(Q_1 Q_2 Q_3 Q_4; g_1 g_2) \rightarrow S_{Q_1 \underline{K}_1 K_2} B_{3\mu}^{f_1 f_2}(Q_1 Q_2 Q_3 Q_4; g_2), \quad (3.39)$$

$$B_{4\mu}^{f_1 f_2}(Q_1 Q_2 Q_3 Q_4; g_1 g_2) \rightarrow S_{Q_3 \underline{K}_1 K_2} B_{4\mu}^{f_1 f_2}(Q_1 Q_2 Q_3 Q_4; g_2), \quad (3.40)$$

$$B_{5\mu}^{f_1 f_2}(Q_1 Q_2 Q_3 Q_4; g_1 g_2) \rightarrow S_{Q_1 \underline{K}_1 Q_2} B_{5\mu}^{f_1 f_2}(Q_1 Q_2 Q_3 Q_4; g_2), \quad (3.41)$$

$$B_{6\mu}^{f_1 f_2}(Q_1 Q_2 Q_3 Q_4; g_1 g_2) \rightarrow S_{Q_1 \underline{K}_1 K_2} B_{6\mu}^{f_1 f_2}(Q_1 Q_2 Q_3 Q_4; g_2); \quad (3.42)$$

the limit when  $g_2$  becomes soft:

$$B_{1\mu}^{f_1 f_2}(Q_1 Q_2 Q_3 Q_4; g_1 g_2) \rightarrow S_{K_1 \underline{K_2} Q_2} B_{1\mu}^{f_1 f_2}(Q_1 Q_2 Q_3 Q_4; g_1), \quad (3.43)$$

$$B_{2\mu}^{f_1 f_2}(Q_1 Q_2 Q_3 Q_4; g_1 g_2) \rightarrow S_{Q_3 \underline{K_2} Q_2} B_{2\mu}^{f_1 f_2}(Q_1 Q_2 Q_3 Q_4; g_1), \quad (3.44)$$

$$B_{3\mu}^{f_1 f_2}(Q_1 Q_2 Q_3 Q_4; g_1 g_2) \rightarrow S_{K_1 \underline{K_2} Q_4} B_{3\mu}^{f_1 f_2}(Q_1 Q_2 Q_3 Q_4; g_1), \quad (3.45)$$

$$B_{4\mu}^{f_1 f_2}(Q_1 Q_2 Q_3 Q_4; g_1 g_2) \rightarrow S_{K_1 \underline{K_2} Q_4} B_{3\mu}^{f_1 f_2}(Q_1 Q_2 Q_3 Q_4; g_1), \quad (3.46)$$

$$B_{5\mu}^{f_1 f_2}(Q_1 Q_2 Q_3 Q_4; g_1 g_2) \rightarrow S_{Q_3 \underline{K_2} Q_4} B_{4\mu}^{f_1 f_2}(Q_1 Q_2 Q_3 Q_4; g_1), \quad (3.47)$$

$$B_{6\mu}^{f_1 f_2}(Q_1 Q_2 Q_3 Q_4; g_1 g_2) \rightarrow S_{K_1 \underline{K_2} Q_2} B_{4\mu}^{f_1 f_2}(Q_1 Q_2 Q_3 Q_4; g_1); \quad (3.48)$$

and the limit when  $g_1$  and  $g_2$  both become soft:

$$B_{1\mu}^{f_1 f_2}(Q_1 Q_2 Q_3 Q_4; g_1 g_2) \rightarrow S_{Q_3 \underline{K_1 K_2} Q_2} B_{\mu}^{f_1 f_2}(Q_1 Q_2 Q_3 Q_4), \quad (3.49)$$

$$B_{2\mu}^{f_1 f_2}(Q_1 Q_2 Q_3 Q_4; g_1 g_2) \rightarrow S_{Q_1 \underline{K_1} Q_4} S_{Q_3 \underline{K_2} Q_2} B_{\mu}^{f_1 f_2}(Q_1 Q_2 Q_3 Q_4), \quad (3.50)$$

$$B_{3\mu}^{f_1 f_2}(Q_1 Q_2 Q_3 Q_4; g_1 g_2) \rightarrow S_{Q_1 \underline{K_1 K_2} Q_4} B_{\mu}^{f_1 f_2}(Q_1 Q_2 Q_3 Q_4), \quad (3.51)$$

$$B_{4\mu}^{f_1 f_2}(Q_1 Q_2 Q_3 Q_4; g_1 g_2) \rightarrow S_{Q_3 \underline{K_1 K_2} Q_4} B_{\mu}^{f_1 f_2}(Q_1 Q_2 Q_3 Q_4), \quad (3.52)$$

$$B_{5\mu}^{f_1 f_2}(Q_1 Q_2 Q_3 Q_4; g_1 g_2) \rightarrow S_{Q_1 \underline{K_1} Q_2} S_{Q_3 \underline{K_2} Q_4} B_{\mu}^{f_1 f_2}(Q_1 Q_2 Q_3 Q_4), \quad (3.53)$$

$$B_{6\mu}^{f_1 f_2}(Q_1 Q_2 Q_3 Q_4; g_1 g_2) \rightarrow S_{Q_1 \underline{K_1 K_2} Q_2} B_{\mu}^{f_1 f_2}(Q_1 Q_2 Q_3 Q_4). \quad (3.54)$$

The soft factors are given by [8]:

$$S_{Q \underline{K} P} = \frac{Q \cdot F \cdot P}{Q \cdot K K \cdot P} \quad (3.55)$$

$$S_{Q \underline{K_1 K_2} P} = \frac{Q \cdot F_1 \cdot F_2 \cdot P}{Q \cdot K_1 K_1 \cdot K_2 K_2 \cdot P} - \frac{Q \cdot F_1 \cdot F_2 \cdot Q}{Q \cdot K_1 K_1 \cdot K_2 (K_1 + K_2) \cdot Q} - \frac{P \cdot F_1 \cdot F_2 \cdot P}{P \cdot (K_1 + K_2) K_1 \cdot K_2 K_2 \cdot P}. \quad (3.56)$$

The following collinear limit was tested: when  $Q_3 \rightarrow zK$ ,  $Q_4 \rightarrow (1-z)K$  with  $K$  an arbitrary lightlike momentum and  $0 < z < 1$ :

$$B_{1\mu}^{f_1 f_2} \rightarrow \frac{1}{2} \sum_{\lambda=\pm 1} h_{\lambda}(\lambda_{q_3}, \lambda_{\bar{q}_4}) S_{\mu}^{f_1 f_2}(Q_1; K\lambda, 1, 2; Q_2) \quad (3.57)$$

$$B_{2\mu}^{f_1 f_2} \rightarrow \frac{1}{2} \sum_{\lambda=\pm 1} h_{\lambda}(\lambda_{q_3}, \lambda_{\bar{q}_4}) S_{\mu}^{f_1 f_2}(Q_1; 1, K\lambda, 2; Q_2) \quad (3.58)$$

$$B_{3\mu}^{f_1 f_2} \rightarrow \frac{1}{2} \sum_{\lambda=\pm 1} h_{\lambda}(\lambda_{q_3}, \lambda_{\bar{q}_4}) S_{\mu}^{f_1 f_2}(Q_1; 1, 2, K\lambda; Q_2) \quad (3.59)$$

$$B_{4\mu}^{f_1 f_2} \rightarrow 0 \quad (3.60)$$

$$B_{5\mu}^{f_1 f_2} \rightarrow 0 \quad (3.61)$$

$$B_{6\mu}^{f_1 f_2} \rightarrow \frac{1}{2} \sum_{\lambda=\pm 1} h_{\lambda}(\lambda_{q_3}, \lambda_{\bar{q}_4}) \{ S_{\mu}^{f_1 f_2}(Q_1; K\lambda, 1, 2; Q_2) + S_{\mu}^{f_1 f_2}(Q_1; 1, K\lambda, 2; Q_2) + S_{\mu}^{f_1 f_2}(Q_1; 1, 2, K\lambda; Q_2) \} \quad (3.62)$$

The collinearity factors can be found in [7].

As a final point of this section we discuss the matrix element squared. To do the colour summation, we write

$$\hat{T}_\mu = \sum_{i=1}^{48} \gamma_i A_{i\mu} \quad (3.63)$$

with, for  $i = 1, \dots, 6$ :

$$\gamma_i = \gamma_i(c_1 c_2 c_3 c_4; a_1 a_2) \text{ as in eqs. (3.4)-(3.9)} \quad (3.64)$$

and

$$A_{i\mu} = ie g^4 \delta^{f_3 f_4} B_{i\mu}^{f_1 f_2}(Q_1 Q_2 Q_3 Q_4; 12). \quad (3.65)$$

For  $i = 7, \dots, 48$ ,  $\gamma_i$  and  $A_{i\mu}$  are given by:

$$\begin{aligned} \gamma_{i+6} &= \gamma_i(a_1 \leftrightarrow a_2), & A_{i+6\mu} &= A_{i\mu}(g_1 \leftrightarrow g_2) & i &= 1, \dots, 6 \\ \gamma_{i+12} &= -\gamma_i(c_1 \leftrightarrow c_3), & A_{i+12\mu} &= A_{i\mu}(Q_1 \leftrightarrow Q_3) & i &= 1, \dots, 12 \\ \gamma_{i+24} &= \gamma_i(c_1 \leftrightarrow c_3, c_2 \leftrightarrow c_4), & A_{i+24\mu} &= A_{i\mu}(Q_1 \leftrightarrow Q_3, Q_2 \leftrightarrow Q_4) & i &= 1, \dots, 12 \\ \gamma_{i+36} &= -\gamma_i(c_2 \leftrightarrow c_4), & A_{i+36\mu} &= A_{i\mu}(Q_2 \leftrightarrow Q_4) & i &= 1, \dots, 12. \end{aligned} \quad (3.66)$$

Using this notation, the colour summed matrix element squared can be written as:

$$\sum_{\text{colour } s} |\mathcal{M}|^2 = \sum_{i=1}^{48} \sum_{j=1}^{48} c_{ij} (V^\mu A_{i\mu})^* (V^\nu A_{j\nu}) \quad (3.67)$$

with

$$c_{ij} = \sum_{c_1 c_2 c_3 c_4 a_1 a_2} \gamma_i^*(c_1 c_2 c_3 c_4 a_1 a_2) \gamma_j(c_1 c_2 c_3 c_4 a_1 a_2). \quad (3.68)$$

The matrix  $c_{ij}$  can be expressed as a rational function of  $N$  using eq. (2.10). For completeness it is given explicitly in appendix Appendix A. Then eq. (3.67) must be summed over all possible helicity combinations.

## 4 Matrix elements with three quark pairs

The matrix element for subprocesses involving six quarks and a vector boson, which decays into a lepton pair, is given by:



$$\mathcal{M} = V^\mu \hat{U}_\mu, \tag{4.1}$$

where  $\hat{U}_\mu$  is the six quark current. Again all the quarks and antiquarks are outgoing particles. We denote the quarks by  $q_1, q_3$  and  $q_5$  and the antiquarks by  $\bar{q}_2, \bar{q}_4$  and  $\bar{q}_6$ . Each of these particles has a momentum  $Q_i$ , a helicity  $\lambda_i$ , a colour  $c_i$  and a flavour  $f_i$ .

$\hat{U}_\mu$  is the sum of nine basic Feynman diagrams and all those which arise by permuting the quarks and the antiquarks. We write

$$\hat{U}_\mu(123456) = \sum_{P(135), P'(246)} (-1)^P (-1)^{P'} \left\{ \frac{1}{2} \hat{m}_{1\mu} + \hat{m}_{2\mu} + \hat{m}_{3\mu} + \hat{m}_{4\mu} \right\}. \tag{4.2}$$

We sum over all quark permutations  $P$  and antiquark permutations  $P'$ . The quantities  $\hat{m}_{i\mu}$  represent the following diagrams:

$$\hat{m}_1 = \begin{array}{c} \begin{array}{c} 4 \\ \downarrow \\ \text{---} \end{array} \\ \begin{array}{c} 1 \\ \downarrow \\ \text{---} \\ \mu \\ \text{---} \\ 2 \\ \downarrow \\ \text{---} \end{array} \end{array} + \begin{array}{c} \begin{array}{c} 4 \\ \downarrow \\ \text{---} \end{array} \\ \begin{array}{c} 1 \\ \downarrow \\ \text{---} \\ \mu \\ \text{---} \\ 2 \\ \downarrow \\ \text{---} \end{array} \end{array} \tag{4.3}$$

$$\hat{m}_2 = \begin{array}{c} \begin{array}{c} 5 \\ \downarrow \\ \text{---} \\ 6 \\ \downarrow \\ \text{---} \end{array} \\ \begin{array}{c} 4 \\ \downarrow \\ \text{---} \\ 3 \\ \downarrow \\ \text{---} \\ 2 \\ \downarrow \\ \text{---} \\ \mu \\ \text{---} \\ 1 \\ \downarrow \\ \text{---} \end{array} \end{array} + \begin{array}{c} \begin{array}{c} 5 \\ \downarrow \\ \text{---} \\ 6 \\ \downarrow \\ \text{---} \end{array} \\ \begin{array}{c} 4 \\ \downarrow \\ \text{---} \\ 3 \\ \downarrow \\ \text{---} \\ 2 \\ \downarrow \\ \text{---} \\ \mu \\ \text{---} \\ 1 \\ \downarrow \\ \text{---} \end{array} \end{array} \tag{4.4}$$

$$\hat{m}_3 = \begin{array}{c} \begin{array}{c} 1 \\ \downarrow \\ \text{---} \\ \mu \\ \text{---} \\ 2 \\ \downarrow \\ \text{---} \end{array} \\ \begin{array}{c} 4 \\ \downarrow \\ \text{---} \\ 3 \\ \downarrow \\ \text{---} \\ 6 \\ \downarrow \\ \text{---} \\ 5 \\ \downarrow \\ \text{---} \end{array} \end{array} + \begin{array}{c} \begin{array}{c} 1 \\ \downarrow \\ \text{---} \\ \mu \\ \text{---} \\ 2 \\ \downarrow \\ \text{---} \end{array} \\ \begin{array}{c} 4 \\ \downarrow \\ \text{---} \\ 3 \\ \downarrow \\ \text{---} \\ 6 \\ \downarrow \\ \text{---} \\ 5 \\ \downarrow \\ \text{---} \end{array} \end{array} \tag{4.5}$$

$$\hat{m}_4 = \begin{array}{c} \begin{array}{c} 5 \\ \downarrow \\ \text{---} \\ 6 \\ \downarrow \\ \text{---} \end{array} \\ \begin{array}{c} 2 \\ \downarrow \\ \text{---} \\ \mu \\ \text{---} \\ 1 \\ \downarrow \\ \text{---} \\ 4 \\ \downarrow \\ \text{---} \\ 3 \\ \downarrow \\ \text{---} \end{array} \end{array} + \begin{array}{c} \begin{array}{c} 5 \\ \downarrow \\ \text{---} \\ 6 \\ \downarrow \\ \text{---} \end{array} \\ \begin{array}{c} 2 \\ \downarrow \\ \text{---} \\ \mu \\ \text{---} \\ 1 \\ \downarrow \\ \text{---} \\ 4 \\ \downarrow \\ \text{---} \\ 3 \\ \downarrow \\ \text{---} \end{array} \end{array}$$

$$+ \begin{array}{c} 5 \quad 2 \quad 1 \quad 4 \\ \downarrow \quad \downarrow \quad \downarrow \quad \downarrow \\ \text{---} \text{---} \text{---} \text{---} \text{---} \\ \uparrow \quad \uparrow \quad \uparrow \quad \uparrow \\ 6 \quad \quad \quad \quad 3 \end{array} \quad (4.6)$$

The quantity  $\hat{m}_{1\mu}$  obtains a factor of  $\frac{1}{2}$  because the diagrams of  $\hat{m}_{1\mu}$  do not change when  $(3 \leftrightarrow 5)$  and  $(4 \leftrightarrow 6)$  are interchanged at the same time. This means that they occur twice in the sum over all the permutations. Extracting some overall factors and the colour factors, we obtain:

$$\hat{m}_{1\mu}(123456) = \frac{1}{4}ieg^4 \{ \delta_{c_1c_4} \delta_{c_3c_6} \delta_{c_5c_2} m_{1\mu}(123456) + \delta_{c_1c_6} \delta_{c_3c_2} \delta_{c_5c_4} m_{1\mu}(125634) \} \quad (4.7)$$

$$\hat{m}_{2\mu}(123456) = \frac{1}{4}ieg^4 \left\{ \delta_{c_1c_6} \delta_{c_3c_2} \delta_{c_5c_4} - \frac{1}{N} \delta_{c_1c_2} \delta_{c_3c_6} \delta_{c_5c_4} - \frac{1}{N} \delta_{c_1c_4} \delta_{c_3c_2} \delta_{c_5c_6} + \frac{1}{N^2} \delta_{c_1c_2} \delta_{c_3c_4} \delta_{c_5c_6} \right\} m_{2\mu}(123456) \quad (4.8)$$

and similar expressions for  $\hat{m}_{3\mu}$  and  $\hat{m}_{4\mu}$ . Substituting them into the formula for  $\hat{U}_\mu$  gives:

$$\hat{U}_\mu = \frac{1}{4}ieg^4 \sum_{P(135)} (-1)^P \delta_{c_1c_6} \delta_{c_3c_2} \delta_{c_5c_4} \left\{ B_{1\mu} + \frac{1}{N} B_{2\mu} + \frac{1}{N^2} B_{3\mu} \right\} \quad (4.9)$$

where  $B_{1\mu}$ ,  $B_{2\mu}$  and  $B_{3\mu}$  are linear combinations of  $m_{1\mu}$ ,  $m_{2\mu}$ ,  $m_{3\mu}$  and  $m_{4\mu}$  with arguments in various different orders. One now has to calculate the  $m_{i\mu}$ 's which will be expressed in smaller objects like  $S_\alpha(Q_1; Q_2)$ .

$$m_{1\mu}(123456) = \delta^{f_3f_4} \delta^{f_5f_6} \frac{S_{\mu\alpha}^{V,f_1f_2}(Q_1; Q_2) S_\beta(Q_3; Q_4) S_\gamma(Q_5; Q_6)}{(Q_3 + Q_4)^2 (Q_5 + Q_6)^2 (Q_3 + Q_4 + Q_5 + Q_6)^2} \times V^{\alpha\beta\gamma}(- (Q_3 + Q_4 + Q_5 + Q_6), Q_3 + Q_4, Q_5 + Q_6). \quad (4.10)$$

For  $m_{2\mu}$ ,  $m_{3\mu}$  and  $m_{4\mu}$  we need some additional building blocks.

$$T_2^{\alpha\beta}(Q_3; Q_4) = \begin{array}{c} 4 \quad 3 \\ \downarrow \quad \downarrow \\ \text{---} \text{---} \text{---} \text{---} \text{---} \\ \uparrow \quad \uparrow \\ \beta \quad \quad \quad \quad \alpha \\ (5+6) \end{array} \quad (4.11)$$

$$T_3^{\alpha\beta}(Q_3; Q_4) = \begin{array}{c} 4 \quad 3 \\ \downarrow \quad \downarrow \\ \text{---} \text{---} \text{---} \text{---} \text{---} \\ \uparrow \quad \uparrow \\ \beta \quad \quad \quad \quad \alpha \\ (5+6) \end{array} \quad (4.12)$$

$$\begin{aligned}
T_{4\mu}^{\alpha\beta V f_1 f_2}(Q_1; Q_2) = & \text{Diagram 1} + \text{Diagram 2} \\
& + \text{Diagram 3}
\end{aligned}
\tag{4.13}$$

The diagrams are Feynman diagrams with external lines labeled  $\beta$ ,  $\alpha$ , 1, 2, and  $\mu$ . Diagram 1:  $\beta$  (left),  $\alpha$  (right), 1 (top), 2 (top),  $\mu$  (top). Diagram 2:  $\beta$  (left),  $\alpha$  (right), 1 (top), 2 (top),  $\mu$  (top). Diagram 3:  $\beta$  (left),  $\alpha$  (right), 1 (top), 2 (top),  $\mu$  (top).

or equivalently,

$$\begin{aligned}
T_2^{\alpha\beta}(Q_3; Q_4) &= J(Q_3)\gamma^\alpha[\mathcal{Q}_4 + \mathcal{Q}_5 + \mathcal{Q}_6]^{-1}\gamma^\beta J(Q_4) \\
T_3^{\alpha\beta}(Q_3; Q_4) &= -J(Q_3)\gamma^\alpha[\mathcal{Q}_3 + \mathcal{Q}_5 + \mathcal{Q}_6]^{-1}\gamma^\beta J(Q_4) \\
T_{4\mu}^{\alpha\beta}(Q_1; Q_2) &= J(Q_1)\Gamma_\mu^{V, f_1 f_2}[\mathcal{Q}_2 + \mathcal{Q}_3 + \mathcal{Q}_4 + \mathcal{Q}_5 + \mathcal{Q}_6]^{-1}\gamma_\alpha[\mathcal{Q}_2 + \mathcal{Q}_5 + \mathcal{Q}_6]^{-1}\gamma^\beta J(Q_2) \\
&\quad - J(Q_1)\gamma^\alpha[\mathcal{Q}_1 + \mathcal{Q}_3 + \mathcal{Q}_4]^{-1}\Gamma_\mu^{V, f_1 f_2}[\mathcal{Q}_2 + \mathcal{Q}_5 + \mathcal{Q}_6]^{-1}\gamma^\beta J(Q_2) \\
&\quad + J(Q_1)\gamma^\alpha[\mathcal{Q}_1 + \mathcal{Q}_3 + \mathcal{Q}_4]^{-1}\gamma^\beta[\mathcal{Q}_1 + \mathcal{Q}_3 + \mathcal{Q}_4 + \mathcal{Q}_5 + \mathcal{Q}_6]^{-1}\Gamma_\mu^{V, f_1 f_2} J(Q_2).
\end{aligned}$$

$$m_{2\mu} = \frac{\delta f_3 f_4 \delta f_5 f_6 S_{\mu\alpha}^{V, f_1 f_2}(Q_1; Q_2) T_2^{\alpha\beta}(Q_3; Q_4) S_\beta(Q_5; Q_6)}{(\mathcal{Q}_5 + \mathcal{Q}_6)^2 (\mathcal{Q}_3 + \mathcal{Q}_4 + \mathcal{Q}_5 + \mathcal{Q}_6)^2}
\tag{4.14}$$

$$m_{3\mu} = \frac{\delta f_3 f_4 \delta f_5 f_6 S_\alpha(Q_5; Q_6) T_3^{\alpha\beta}(Q_3; Q_4) S_{\mu\beta}^{V, f_1 f_2}(Q_1; Q_2)}{(\mathcal{Q}_5 + \mathcal{Q}_6)^2 (\mathcal{Q}_3 + \mathcal{Q}_4 + \mathcal{Q}_5 + \mathcal{Q}_6)^2}
\tag{4.15}$$

$$m_{4\mu} = \frac{\delta f_3 f_4 \delta f_5 f_6 S_\alpha(Q_3; Q_4) T_{4\mu}^{\alpha\beta}(Q_1; Q_2) S_\beta(Q_5; Q_6)}{(\mathcal{Q}_3 + \mathcal{Q}_4)^2 (\mathcal{Q}_5 + \mathcal{Q}_6)^2}
\tag{4.16}$$

Now we use Weyl-van der Waerden spinors to calculate the  $m_{i\mu}$ 's for the helicity combination  $(\lambda_1 \lambda_2 \lambda_3 \lambda_4 \lambda_5 \lambda_6) = (+ - + - + -)$ . Once they are known, the  $m_{i\mu}$ 's for other helicities can easily be derived. This is done as follows. First note some properties of the currents  $T_2^{\alpha\beta}$ ,  $T_3^{\alpha\beta}$  and  $S_\alpha$ :

$$\begin{aligned}
S_\alpha(Q_3 \lambda_3; Q_4 \lambda_4) &= S_\alpha(Q_4 \lambda_4; Q_3 \lambda_3) \\
T_3^{\alpha\beta}(Q_3 \lambda_3; Q_4 \lambda_4) &= -T_2^{\beta\alpha}(Q_4 \lambda_4; Q_3 \lambda_3).
\end{aligned}
\tag{4.17}$$

From these properties the following relations can be derived.

$$\begin{aligned}
m_{1\mu}(\lambda_1 \lambda_2 - + \lambda_5 \lambda_6) &= m_{1\mu}(\lambda_1 \lambda_2 + - \lambda_5 \lambda_6, Q_3 \leftrightarrow Q_4) \\
m_{1\mu}(\lambda_1 \lambda_2 \lambda_3 \lambda_4 - +) &= m_{1\mu}(\lambda_1 \lambda_2 \lambda_3 \lambda_4 + -, Q_5 \leftrightarrow Q_6)
\end{aligned}$$

$$\begin{aligned}
m_{2\mu}(\lambda_1\lambda_2 - +\lambda_5\lambda_6) &= -m_{3\mu}(\lambda_1\lambda_2 + -\lambda_5\lambda_6, Q_3 \leftrightarrow Q_4) \\
m_{2\mu}(\lambda_1\lambda_2\lambda_3\lambda_4 - +) &= m_{2\mu}(\lambda_1\lambda_2\lambda_3\lambda_4 + -, Q_5 \leftrightarrow Q_6) \\
m_{3\mu}(\lambda_1\lambda_2 - +\lambda_5\lambda_6) &= -m_{2\mu}(\lambda_1\lambda_2 + -\lambda_5\lambda_6, Q_3 \leftrightarrow Q_4) \\
m_{3\mu}(\lambda_1\lambda_2\lambda_3\lambda_4 - +) &= m_{3\mu}(\lambda_1\lambda_2\lambda_3\lambda_4 + -, Q_5 \leftrightarrow Q_6) \\
m_{4\mu}(\lambda_1\lambda_2 - +\lambda_5\lambda_6) &= m_{4\mu}(\lambda_1\lambda_2 + -\lambda_5\lambda_6, Q_3 \leftrightarrow Q_4) \\
m_{4\mu}(\lambda_1\lambda_2\lambda_3\lambda_4 - +) &= m_{4\mu}(\lambda_1\lambda_2\lambda_3\lambda_4 + -, Q_5 \leftrightarrow Q_6)
\end{aligned} \tag{4.18}$$

To get the helicity combinations with  $(\lambda_1\lambda_2) = (-+)$ , we use complex conjugation.

$$\begin{aligned}
m_{i\mu}(-, +, \lambda_3, \lambda_4, \lambda_5, \lambda_6) &= \\
[m_{i\mu}(+, -, -\lambda_3, -\lambda_4, -\lambda_5, -\lambda_6, R^{V, f_1 f_2} \rightarrow L^{V, f_1 f_2})]^*
\end{aligned} \tag{4.19}$$

These rules are sufficient to obtain all other helicity amplitudes.

In order to square the matrix element one introduces an amplitude  $X(P)$  depending on a specific permutation  $P$  of the quarks.

$$\mathcal{M} = V^\mu \hat{U}_\mu = \frac{1}{4} i e g^4 \sum_{P(135)} (-1)^P X(P) \delta_{c_{P(1)}c_6} \delta_{c_{P(3)}c_2} \delta_{c_{P(5)}c_4} \tag{4.20}$$

with

$$\begin{aligned}
X(P) &= V^\mu \left\{ B_{1\mu}(P(1)2P(3)4P(5)6) \right. \\
&\quad \left. + \frac{1}{N} B_{2\mu}(P(1)2P(3)4P(5)6) + \frac{1}{N^2} B_{3\mu}(P(1)2P(3)4P(5)6) \right\}
\end{aligned} \tag{4.21}$$

The six quark orderings (135), (153), (351), (315), (513) and (531) are obtained by permutations  $P_i$  ( $i = 1, \dots, 6$ ) from the ordering (135). Summing over the colours leads to a  $6 \times 6$  colour matrix  $c_{PP'}$ .

$$\sum_{c_1 \dots c_6} |\mathcal{M}|^2 = \left( \frac{e g^4}{4} \right)^2 \sum_P \sum_{P'} c_{PP'} X(P)^* X(P') \tag{4.22}$$

with

$$c_{PP'} = \begin{pmatrix} N^3 & -N^2 & N & -N^2 & N & -N^2 \\ -N^2 & N^3 & -N^2 & N & -N^2 & N \\ N & -N^2 & N^3 & -N^2 & N & -N^2 \\ -N^2 & N & -N^2 & N^3 & -N^2 & N \\ N & -N^2 & N & -N^2 & N^3 & -N^2 \\ -N^2 & N & -N^2 & N & -N^2 & N^3 \end{pmatrix} \tag{4.23}$$

Of course one still has to sum over all the helicities in eq. (4.22).

When one restricts the calculations to  $W$  production a number of simplifications occur, both in the four and in the six quark cases. Since  $R^{W, f_1 f_2} = 0$ , all helicity amplitudes with  $(\lambda_{q_1}, \lambda_{q_2}) = (+-)$

vanish. Knowing the quark flavours, the Kronecker delta in eq. (3.11) reduces the number of quark permutations that contribute to  $\mathcal{M}$ .

In the four quark case at least two quarks must have the same flavour. By rearranging the particles we label them as  $q_3$  and  $\bar{q}_4$ . Then  $q_1$  and  $\bar{q}_2$  must have different flavours. So we have  $f_1 \neq f_2, f_3 = f_4$ . This leaves three possible situations.

1).  $f_1 \neq f_3, f_2 \neq f_3$ , eg.  $u\bar{d}c\bar{c}$ . In this case, no quark permutations are allowed:

$$\hat{T}_\mu(Q_1Q_2Q_3Q_4; 12) = \hat{A}_\mu(Q_1Q_2Q_3Q_4; 12). \quad (4.24)$$

2).  $f_1 = f_3 = f_4 \neq f_2$ , eg.  $u\bar{d}u\bar{u}$ . Now  $q_1$  and  $q_3$  are identical particles, so

$$\hat{T}_\mu(Q_1Q_2Q_3Q_4; 12) = \hat{A}_\mu(Q_1Q_2Q_3Q_4; 12) - \hat{A}_\mu(Q_3Q_2Q_1Q_4; 12). \quad (4.25)$$

3).  $f_1 \neq f_2 = f_3 = f_4$ , eg.  $u\bar{d}d\bar{d}$ . Here

$$\hat{T}_\mu(Q_1Q_2Q_3Q_4; 12) = \hat{A}_\mu(Q_1Q_2Q_3Q_4; 12) - \hat{A}_\mu(Q_1Q_4Q_3Q_2; 12). \quad (4.26)$$

Our computer program produces three different  $|\mathcal{M}|^2$ 's, one for each type of flavour combination. The  $|\mathcal{M}|^2$  for case 2) does not change when  $q_1 \leftrightarrow q_3$ . In case 3), it does not change when  $\bar{q}_2 \leftrightarrow \bar{q}_4$ . In all three cases  $|\mathcal{M}|^2$  is invariant under  $g_1 \leftrightarrow g_2$ . These symmetries were checked numerically.

In the six quark case there are seven types of flavour combinations. In all seven combinations we have  $f_1 \neq f_2, f_3 = f_4$  and  $f_5 = f_6$ .

1).  $f_1, f_2, f_3, f_5$  all different, eg.  $u\bar{d}c\bar{c}b\bar{b}$ .

2).  $f_3 = f_5$ , eg.  $u\bar{d}c\bar{c}c\bar{c}$ .

3).  $f_1 = f_3$ , eg.  $u\bar{d}u\bar{u}c\bar{c}$ .

4).  $f_2 = f_5$ , eg.  $u\bar{d}c\bar{c}d\bar{d}$ .

5).  $f_1 = f_3, f_2 = f_5$ , eg.  $u\bar{d}u\bar{u}d\bar{d}$ .

6).  $f_1 = f_3 = f_5$  eg.  $u\bar{d}u\bar{u}u\bar{u}$ .

7).  $f_2 = f_3 = f_5$  eg.  $u\bar{d}d\bar{d}d\bar{d}$ .

Many symmetries exist for these cases. Like in the four quark case we have checked them numerically.

## 5 Numerical results

In this section we present cross sections for the production of  $l\nu + (2, 3, 4)$  jets for Fermilab, LHC and SSC energies. Moreover we compare this cross section with the top pair production cross section with the subsequent decay of the top pair  $t\bar{t} \rightarrow W^+W^- b\bar{b} \rightarrow l\nu + (2, 3, 4)$  jets. As mentioned in the introduction this is one of the important processes in which the top quark can be found.

Collider	FNAL	LHC	SSC
$\sqrt{s}$ (TeV)	1.8	16	40
Struc. Func.	MRSEB	MRSEB	MRSEB
QCD scale	$M_W$	$M_W$	$M_W$
$E_t^{\min}(j)$ (GeV)	15	50	50
$ \eta^{\max}(j) $	2.0	3.0	3.0
$\Delta R^{\min}(j, j)$	*	0.4	0.4
$E_t^{\min}(l)$ (GeV)	20	50	50
$E_t^{\min}(\text{mis})$ (GeV)	20	50	50
$ \eta^{\max}(l) $	1.0	3.0	3.0
$\Delta R^{\min}(j, l)$	0.0	0.4	0.4

Table 3. Structure functions, QCD scale and cuts used for each collider throughout this section. (\* means defined in text.)

number of jets	2 quarks	4 quarks	6 quarks	total
0	745	-	-	745
1	130	-	-	130
2	21.5	4.5	-	26.0
3	3.4	1.44	-	4.8
4	0.40	0.30	0.0131	0.71

Table 4. The  $P\bar{P} \rightarrow W + \text{jets}$  cross section (in picobarn) for Fermilab ( $\Delta R(j, j) > 0.7$ ) divided in subprocesses depending on the number of quarks in the process.

Therefore the comparison between the signal and the background is crucial for the ability to find the top quark in the lepton plus jets decay channel. In a later paper we will study the possibility of finding the top quark in this decay mode in greater detail. For the super colliders both the top signal and the  $W$  production are a background to the Higgs search in this decay channel.

$R_n$	$\Delta R(j, j) > 0.4$	$\Delta R(j, j) > 0.7$	$\Delta R(j, j) > 1.4$
(1)	(0.17)	(0.17)	(0.17)
2	0.22	0.20	0.16
3	0.22	0.18	0.11
4	0.22	0.15	0.07

Table 5. The ratio  $R_n$  for several  $\Delta R(j, j)$  cuts at Fermilab energies.

$m_{\text{top}}$ (GeV)	$\sigma(l\nu + 2 \text{ jets})$	$\sigma(l\nu + 3 \text{ jets})$	$\sigma(l\nu + 4 \text{ jets})$
90	5.47	2.61	0.23
100	2.74	3.97	1.33
110	0.998	2.60	1.70
120	0.445	1.61	1.44
130	0.235	1.02	1.10
140	0.135	0.669	0.818
150	0.084	0.452	0.601
160	0.053	0.314	0.445
170	0.036	0.222	0.330
180	0.024	0.159	0.245
190	0.017	0.115	0.183
200	0.012	0.085	0.162
background	26.0	4.8	0.71
with tagging	0.27	0.087	0.022

Table 6. The  $P\bar{P} \rightarrow t\bar{t} \rightarrow l\nu + (2,3,4)$  jet cross sections (in picobarn) for various top masses (in GeV) and the  $P\bar{P} \rightarrow W + \text{jets}$  background with and without b-tagging at Fermilab energies ( $\Delta R(j, j) > 0.7$ ).

The results also serve as a check of the Monte Carlo program, which uses the matrix elements of this paper. Of course the tests described in the previous sections were carried out, i.e. soft and collinear behaviour, current conservation, charge conjugation and equal quark flavour symmetries. The ratio

$$R_n = \sigma(W + n \text{ jets}) / \sigma(W + (n - 1) \text{ jets}) \quad (5.1)$$

offers a good possibility for a final check on the program.

Before presenting and discussing the results we specify the input needed for the numerical calculations. The cuts and parameters used are given in table 3. The minimal transverse energy  $E_t^{\min}(j)$ , maximum pseudorapidity  $|\eta^{\max}(j)|$  and the minimum separation  $\Delta R^{\min}(j, j)$  are the cuts on the outgoing partons. The separation  $\Delta R$  is defined as

$$\Delta R = \sqrt{(\Delta\Phi)^2 + (\Delta\eta)^2}, \quad (5.2)$$

where  $\Delta\Phi$  is the difference in the azimuthal angle and  $\Delta\eta$  the difference in rapidity between two partons. In terms of a  $\Phi, \eta$  lego-plot,  $\Delta R$  is the distance between two partons. The lepton cuts are the minimum transverse energy  $E_t^{\min}(l)$  and the maximum pseudorapidity  $|\eta^{\max}(l)|$ . Throughout the paper the lepton  $l$  is the charged lepton and we consider only the  $e^\pm$  signal. The cross sections are the sum of the  $W^+$  and  $W^-$  cross sections. The minimal required missing energy is  $E_t^{\min}(\text{mis})$ . Finally a minimal separation of lepton and parton of  $\Delta R^{\min}(j, l)$  is imposed.

$m_{\text{top}}$ (GeV)	$\sigma(l\nu + 2 \text{ jets})$	$\sigma(l\nu + 3 \text{ jets})$	$\sigma(l\nu + 4 \text{ jets})$
100	37.9	7.9	0.48
110	34.0	10.7	1.27
120	29.8	11.4	1.72
130	25.4	11.6	2.10
140	21.5	11.4	2.28
150	18.3	11.2	2.38
160	15.7	10.7	2.40
170	13.4	10.2	2.41
180	11.1	9.82	2.48
190	9.22	9.38	2.49
200	7.51	8.81	2.51
background	52	24	8.7
with tagging	0.087	0.24	0.17

Table 7. The  $PP \rightarrow t\bar{t} \rightarrow l\nu + (2,3,4)$  jet cross sections (in picobarn) for various top masses (in GeV) and the  $PP \rightarrow W + \text{jets}$  background with and without b-tagging at LHC energies

The used parton distributions are the MRSEB structure functions [9] ( $\Lambda_{\overline{\text{MS}}} = 200 \text{ MeV}$ ) with the QCD scale  $Q = M_W$ . Since we are mainly interested in a global study of some cross sections we did not look at detailed issues like the scale and structure function dependence of the results. We postpone this to a later paper. The Monte Carlo of ref. [10] is used to generate the top signal cross sections with the QCD scale chosen to be equal to the top mass. In table 4 we use cuts which more or less typify the CDF-detector.

Turning to the results, we first discuss the relative importance of various subprocesses for the measurements at the Tevatron. Table 4 gives the total cross section as well as the separate contributions from the subprocesses according to the number of quarks involved in the process. We notice that processes with four quarks become more and more important compared to the two quark subprocesses for an increasing number of jets. For 2, 3 and 4 jets respectively 17%, 30% and 42% of the total cross section comes from the four quark subprocesses. This implies that the fraction of the jets which are quark jets increases with an increasing number of jets. Note further that the six quark subprocess (i.e.  $qq \rightarrow qq\bar{q}qW$ ) is negligible, the contribution to the total cross section is only 1.8%.

Next we discuss the behaviour of  $R_n$  as defined in eq. (5.1). As was conjectured in ref. [11] and later verified for up to 3 jets [6], the ratio  $R_n$  is approximately constant for reasonable cuts. For loose CDF cuts (see table 3, with  $\Delta R(j, j) > 0.7$ ) this ratio is roughly 1/5. Of course there is a limit on the validity of this rule of thumb. This shows up easily when considering the available phase space for the extra jet in the ratio. With an increasing number of jets, the available phase space for adding a jet quickly decreases. Since it eventually becomes impossible to add another



$m_{\text{top}}$ (GeV)	$\sigma(l\nu + 2 \text{ jets})$	$\sigma(l\nu + 3 \text{ jets})$	$\sigma(l\nu + 4 \text{ jets})$
100	179	39.6	2.3
110	165	54.4	6.5
120	146	59.6	9.4
130	127	62.2	11.9
140	112	62.9	13.2
150	97.6	62.4	14.0
160	84.8	61.6	14.6
170	74.2	59.4	15.1
180	63.6	58.0	15.5
190	54.3	55.9	15.6
200	45.9	53.2	15.8
background	177	107	46
with tagging	0.21	1.0	1.0

Table 8. The  $PP \rightarrow t\bar{t} \rightarrow l\nu + (2,3,4)$  jet cross sections (in picobarn) for various top masses (in GeV) and the  $P\bar{P} \rightarrow W + \text{jets}$  background with and without b-tagging at SSC energies

jet, this means that the constant ratio rule of thumb must break down for a high number of jets. However if we make the jet “small” (e.g. a small jet cone) the breakdown of the constant ratio rule is postponed. This is demonstrated in table 5. Note that the ratio  $R_1$  is not a relevant quantity in this comparison, since in tree level approximation it is independent of  $\Delta R(j, j)$ . It is only listed for completeness. We see in table 5 that for  $\Delta R^{\min}(j, j) = 0.4$  the ratio is a constant within the numerical accuracy. As expected we see that with increasing  $\Delta R^{\min}(j, j)$  this is no longer the case and the deviation from constant ratio increases with increasing  $\Delta R^{\min}(j, j)$ . The fact that  $R_4 = R_3 = R_2$  for sufficiently small  $\Delta R^{\min}(j, j)$  is a good test on the absolute normalization of the Monte Carlo program.

It is of interest to compare the cross section  $P\bar{P} \rightarrow l\nu + (2,3,4)$  jets with top pair production where each top quark subsequently decays in a b quark and a  $W$ ,  $P\bar{P} \rightarrow b\bar{b}W^+W^-$ . One of the possible decay channels is that one  $W$  decays hadronically into 2 jets and the other one leptonically to give a charged lepton and a (anti)neutrino. The  $E_t$  of the bottom quarks is strongly dependent on the top mass. If the top mass is close to the  $W$  mass the bottom quarks will have, in most of the events, a low transverse energy and will not pass the threshold for recognisable jets [12]. When the top mass increases it becomes more likely that one or both of the bottom quarks will pass the  $E_t^{\min}(j)$  threshold and develops into a jet. For the Tevatron this can be clearly seen in table 6. For  $m_{\text{top}} = 90$  GeV most of the events are with two jets, while the fraction of lepton plus four jet events is the smallest. This in contrast with a heavier top mass. From a mass of 140 GeV onward the situation is reversed and most of the events are with four accompanying jets. The important issue is the relative size of the background compared to the top signal. The top search in the lepton

plus two jet channel were extensively studied in refs. [12]. Since the top mass is above 89 GeV [13] the background is too large to observe the top quark in the two jet mode. The top search in the three jet plus lepton decay was studied in refs. [14]. As can be seen from table 6 the background remains a problem, though compared to the two jet plus lepton mode the signal to background ratio is improved considerably. For the four jet plus lepton mode the signal is larger than the background over a large mass range of the top. This offers a good possibility of finding the top quark in the four jet plus lepton mode. One disadvantage is that the cross sections are of the order 1 picobarn. With an estimated luminosity of  $25 \text{ pb}^{-1}$  from the next Tevatron run we can expect around 18 events from the background, while the top pair signal could give as many as 42 additional events (for a top mass around 110 GeV).

Also included in table 6 is the background when we demand a  $b\bar{b}$  quark pair in the final state. That is it is the cross section for  $P\bar{P} \rightarrow W + (2, 3, 4)$  jets where two of the jets are tagged as  $b$  jets. No efficiency for the tagging is folded in. This  $b$  tagging might become possible at the coming measurement of the CDF collaboration at Fermilab. This opens the possibility for reducing the background to the topsearch in the lepton + jets channel considerably. In fact the top signal has always two  $b$  quarks in the final state though they will not always develop into jets as was already explained and is clearly demonstrated in table 6. Therefore the effect of tagging on the top signal and the  $W$  background depends on the number of jets in the final state.

For the final state  $l\nu + 2$  jets the top signal in this lowest order approximation disappears because both the  $b$  quark as the  $\bar{b}$  quark are soft. The  $W$  background is reduced by a factor 100. Of course we have to include the tagging efficiency  $\epsilon$ . If we demand to see at least one  $b$  tagged jet the efficiency is much higher and is given by  $\epsilon_b = 2\epsilon(1 - \epsilon) + \epsilon^2$ . It is worthwhile to notice that the  $l\nu + 2$  jets can be used in an experiment to test the validity of the tree level calculation with  $b$  tagging, since there is no "top contamination" in this channel.

In the  $l\nu + 3$  jet final state the top signal contributes, though there is only one  $b$  jet in the final state. The background is reduced by a factor of 50. This means that the background is negligible over a wide range of top masses. A disadvantage is that there is only one  $b$  jet in the signal and two  $b$  jets in the background which are affected differently by the efficiency.

This latter phenomenon does not happen in the  $l\nu + 4$  jets final state. From table 6 we see that the cross section is reduced by a factor of 30. This means that the  $W$  background is no problem in the top search. As a simple example assume a top mass of 120 GeV, a tagging efficiency  $\epsilon_b = 20\%$  and a luminosity of  $25 \text{ pb}^{-1}$ . Then the expected number of top events is approximately 7 events and 0.1 background events. This means that seeing  $l\nu + 4$  jet events with at least one tagged  $b$  is almost certainly a top event. With only a handful of events it is then possible to determine the top mass by reconstructing the events in a consistent manner.

For completeness we also include some results on the processes  $PP \rightarrow W + \text{jets}$  and  $PP \rightarrow t\bar{t} \rightarrow l\nu + \text{jets}$  at future super collider energies. The results in tables 7 and 8 give an indication of what to expect. The SSC cross section is roughly a factor 3-5 larger than the LHC cross section for the same cuts. Note further that the ratio  $R_n$  is large for the super colliders (e.g. for the SSC collider  $R_2$  is as high as 0.82). This makes the validity of the treelevel calculation questionable. To get a

more reliable estimate for the cross section (and a  $R_n$  of order 0.2) one should impose tighter cuts on the jets, especially on the  $E_t^{\min(j)}$ . We don't pursue this question here, since we consider the results of tables 7 and 8 as a mere illustration of the presented calculations.

## 6 Summary and conclusions

In this paper it is shown how the complexity of the production of a vector boson and jets increases with the number of jets. In view of the particular relevance of the four jet cross section the exact calculation has here been carried out. For the one quark pair subprocesses recursive techniques can handle the large number of diagrams. For the two quark pairs and three quark pairs explicit Feynman diagram calculations can be carried out when an optimal use is made of the freedom in choice of polarization vectors for the gluons in gauge invariant subamplitudes. As in our previous calculations Weyl-van der Waerden spinor calculus is the tool to obtain the helicity amplitudes.

With these matrix elements inserted in a Monte Carlo program one can have a first global look at some physics results. The program and its matrix elements satisfy the consistency checks we can impose. The signal to background ratios for top search in the  $W$  and four jets channel look promising for the Tevatron and will be further investigated in a separate paper. Also results for LHC and SSC energies are given. The cuts on the jets should here become more tight than at lower energies in order to get more reliable predictions from tree diagram calculations.

## Appendix A The colour matrix for the four quark processes

The  $48 \times 48$  colour matrix  $c$  defined in (3.68) can be written as

$$c = \begin{pmatrix} c_A & c_B & c_C & c_D \\ c_B & c_A & c_D & c_C \\ c_C & c_D & c_A & c_B \\ c_D & c_C & c_B & c_A \end{pmatrix},$$

where

$$c_A = \begin{pmatrix} c_1 & c_2 \\ c_2 & c_1 \end{pmatrix}, c_B = \begin{pmatrix} c_3 & c_4 \\ c_4 & c_3 \end{pmatrix}, c_C = \begin{pmatrix} c_5 & c_6 \\ c_6 & c_5 \end{pmatrix}, c_D = \begin{pmatrix} c_7 & c_8 \\ c_8 & c_7 \end{pmatrix},$$

and

$$c_1 = \begin{pmatrix} \delta_1 & 0 & \delta_2 & -\delta_4 & \delta_3 & -\delta_4 \\ 0 & \delta_1 & 0 & \delta_3 & -\delta_4 & -\delta_4 \\ \delta_2 & 0 & \delta_1 & -\delta_4 & -\delta_4 & -\delta_4 \\ -\delta_4 & \delta_3 & -\delta_4 & \delta_4 & 0 & \delta_3 \\ \delta_3 & -\delta_4 & -\delta_4 & 0 & \delta_4 & 0 \\ -\delta_4 & -\delta_4 & -\delta_4 & \delta_3 & 0 & \delta_4 \end{pmatrix}, c_2 = \begin{pmatrix} -\delta_2 & 0 & \delta_2 & \delta_3 & -\delta_4 & \delta_3 \\ 0 & \delta_2 & 0 & -\delta_4 & -\delta_4 & \delta_3 \\ \delta_2 & 0 & -\delta_2 & \delta_3 & \delta_3 & \delta_3 \\ \delta_3 & -\delta_4 & \delta_3 & -\delta_3 & 0 & \delta_3 \\ -\delta_4 & -\delta_4 & \delta_3 & 0 & \delta_3 & 0 \\ \delta_3 & \delta_3 & \delta_3 & \delta_3 & 0 & -\delta_3 \end{pmatrix},$$

$$c_3 = \begin{pmatrix} -\delta_5 & -\delta_5 & -\delta_5 & \delta_6 & 0 & \delta_5 \\ -\delta_5 & -\delta_5 & \delta_6 & 0 & \delta_6 & 0 \\ -\delta_5 & \delta_6 & -\delta_5 & \delta_5 & 0 & \delta_6 \\ \delta_6 & 0 & \delta_5 & -\delta_7 & -\delta_7 & -\delta_7 \\ 0 & \delta_6 & 0 & -\delta_7 & -\delta_7 & \delta_8 \\ \delta_5 & 0 & \delta_6 & -\delta_7 & \delta_8 & -\delta_7 \end{pmatrix}, c_4 = \begin{pmatrix} \delta_6 & \delta_6 & \delta_6 & \delta_6 & 0 & -\delta_6 \\ \delta_6 & -\delta_5 & -\delta_5 & 0 & \delta_5 & 0 \\ \delta_6 & -\delta_5 & \delta_6 & -\delta_6 & 0 & \delta_6 \\ \delta_6 & 0 & -\delta_6 & \delta_6 & \delta_6 & \delta_6 \\ 0 & \delta_5 & 0 & \delta_6 & -\delta_7 & -\delta_7 \\ -\delta_6 & 0 & \delta_6 & \delta_6 & -\delta_7 & \delta_6 \end{pmatrix},$$

$$c_5 = \begin{pmatrix} \delta_2 & 0 & \delta_1 & -\delta_4 & -\delta_4 & -\delta_4 \\ 0 & \delta_2 & 0 & -\delta_4 & -\delta_4 & \delta_3 \\ \delta_1 & 0 & \delta_2 & -\delta_4 & \delta_3 & -\delta_4 \\ -\delta_4 & -\delta_4 & -\delta_4 & \delta_3 & 0 & \delta_4 \\ -\delta_4 & -\delta_4 & \delta_3 & 0 & \delta_3 & 0 \\ -\delta_4 & \delta_3 & -\delta_4 & \delta_4 & 0 & \delta_3 \end{pmatrix}, c_6 = \begin{pmatrix} \delta_2 & 0 & -\delta_2 & \delta_3 & \delta_3 & \delta_3 \\ 0 & \delta_1 & 0 & \delta_3 & -\delta_4 & -\delta_4 \\ -\delta_2 & 0 & \delta_2 & \delta_3 & -\delta_4 & \delta_3 \\ \delta_3 & \delta_3 & \delta_3 & \delta_3 & 0 & -\delta_3 \\ \delta_3 & -\delta_4 & -\delta_4 & 0 & \delta_4 & 0 \\ \delta_3 & -\delta_4 & \delta_3 & -\delta_3 & 0 & \delta_3 \end{pmatrix},$$

$$c_7 = \begin{pmatrix} -\delta_5 & \delta_6 & -\delta_5 & \delta_5 & 0 & \delta_6 \\ \delta_6 & -\delta_5 & -\delta_5 & 0 & \delta_5 & 0 \\ -\delta_5 & -\delta_5 & -\delta_5 & \delta_6 & 0 & \delta_5 \\ \delta_5 & 0 & \delta_6 & -\delta_7 & \delta_6 & -\delta_7 \\ 0 & \delta_5 & 0 & \delta_6 & -\delta_7 & -\delta_7 \\ \delta_6 & 0 & \delta_5 & -\delta_7 & -\delta_7 & -\delta_7 \end{pmatrix}, c_8 = \begin{pmatrix} \delta_6 & -\delta_5 & \delta_6 & -\delta_6 & 0 & \delta_6 \\ -\delta_5 & -\delta_5 & \delta_6 & 0 & \delta_6 & 0 \\ \delta_6 & \delta_6 & \delta_6 & \delta_6 & 0 & -\delta_6 \\ -\delta_6 & 0 & \delta_6 & \delta_6 & -\delta_7 & \delta_6 \\ 0 & \delta_6 & 0 & -\delta_7 & -\delta_7 & \delta_6 \\ \delta_6 & 0 & -\delta_6 & \delta_6 & \delta_6 & \delta_6 \end{pmatrix}.$$

The constants  $\delta_1 \dots \delta_8$  are given by

$$\delta_i = \frac{N^2 - 1}{4} (N^2 - 1, 1, N^{-2}, 1 - N^{-2}, N - N^{-1}, N^{-1}, N^{-1} - N^{-3}, N^{-3}).$$

## References

- [1] F.A. Berends, W.T. Giele and H. Kuijf, Nucl. Phys. **B321** (1989) 39.
- [2] K. Hagiwara and D. Zeppenfeld, Nucl. Phys. **B313** (1989) 560.
- [3] D. Zeppenfeld, *Private communication*.
- [4] R. Kleiss and W.J. Stirling, Phys. Lett. **200B** (1988) 193.
- [5] J.F. Gunion, H.E. Haber, G.L. Kane and S. Dawson, *Higgs Hunter's Guide*, SCIPP-89/13 (1989).
- [6] F.A. Berends, W.T. Giele, R. Kleiss, H. Kuijf and W.J. Stirling, Phys. Lett. **224B** (1989) 237.
- [7] F.A. Berends and W.T. Giele, Nucl. Phys. **B306** (1988) 91.
- [8] F.A. Berends and W.T. Giele, Nucl. Phys. **B313** (1989) 39.

- [9] A.D. Martin, R.G. Roberts and W.J. Stirling, Phys. Lett. **206B** (1988) 327.
- [10] R. Kleiss and W.J. Stirling, Z. Phys. **C40** (1988) 419.
- [11] S.D. Ellis, R. Kleiss and W.J. Stirling, Phys. Lett. **154B** (1985) 435.
- [12] R. Kleiss, A.D. Martin and W.J. Stirling, Z. Phys. **C39** (1988) 393;  
S. Gupta and D.P. Roy, Z. Phys. **C39** (1988) 417;  
F. Halzen, C.S. Kim and A.D. Martin, Mod. Phys. Lett. **A4** (1989) 1531;  
P. Agrawal and S.D. Ellis, Phys. Lett. **221B** (1989) 393;  
J.L. Rosner, Phys. Rev. D **39** (1989) 3297, Erratum-ibid. **D4** (1989) 1701.
- [13] F. Abe et al, Phys Rev Let **64**:147,1990;  
G.P. Yeh, FERMILAB-CONF-90/138-E, to be published in the proceedings of 'Les Rencontres de Physique de la Vallée d'Aoste', Editions Frontieres (1990), ed. M. Greco.
- [14] H. Baer, V. Barger and R.J.N. Phillips, Phys. Lett. **221B** (1989) 398;  
W.T. Giele and W.J. Stirling, Nucl. Phys. **B343** (1990) 14.